The Astrophysical Journal, 671:1355–1364, 2007 December 20
© 2007. The American Astronomical Society. All rights reserved. Printed in U.S.A.

CHARACTERISTICS OF EGRET BLAZARS IN THE VLBA IMAGING AND POLARIMETRY SURVEY (VIPS)

G. B. Taylor,[1] S. E. Healey,[2] J. F. Helmboldt,[3] S. Tremblay,[1] C. D. Fassnacht,[4] R. C. Walker,[5] L. O. Sjouwerman,[5] T. J. Pearson,[6] A. C. S. Readhead,[6] L. Weintraub,[6] N. Gehrels,[7] R. W. Romani,[2] P. F. Michelson,[2] R. D. Blandford,[8] and G. Cotter[9]

Received 2007 June 3; accepted 2007 September 6

ABSTRACT

We examine the radio properties of EGRET-detected blazars observed as part of the VLBA Imaging and Polarimetry Survey (VIPS). VIPS has a flux limit roughly an order of magnitude below the MOJAVE survey and most other samples that have been used to study the properties of EGRET blazars. At lower flux levels, radio flux density does not directly correlate with gamma-ray flux density. We do find that the EGRET-detected blazars tend to have higher brightness temperatures, greater core fractions, and possibly larger than average jet opening angles. A weak correlation is also found with jet length and with polarization. All of the well-established trends can be explained by systematically larger Doppler factors in the gamma-ray-loud blazars, consistent with the measurements of higher apparent velocities found in monitoring programs carried out at radio frequencies above 10 GHz.

Subject headings: catalogs — galaxies: active — galaxies: jets — galaxies: nuclei — radio continuum: galaxies — surveys — techniques: image processing

1. INTRODUCTION

At high galactic latitudes at least ~70% of the sources seen by the *Compton Gamma-Ray Observatory* (*CGRO*; Hartman et al. 1999) EGRET instrument are identified with blazars (Sowards-Emmerd et al. 2003, 2004, 2005). These blazars exhibit flat radio spectra, rapid variability, compact cores with one-sided parsec-scale jets, and superluminal motion in the jets (Marscher 2006). At optical wavelengths blazars are characterized by broad or no emission lines, optically violently variable behavior, and relatively high linear polarization (Urry & Padovani 1995).

The identified EGRET blazars display a number of interesting radio properties. Based on 22 and 37 GHz monitoring of 43 sources, Lähteenmäki & Valtaoja (2003) suggest that the EGRET flares lagged behind millimeter flares. This is in direct contrast to other studies (e.g., Reich et al. 1993) that claimed enhanced radio emission following a high level of gamma-ray activity. Lister & Homan (2005) find that EGRET blazars have more strongly polarized jets than found in compact objects on average based on analysis of 26 EGRET sources overlapping with the Monitoring of Jets in Active Galactic Nuclei with VLBA Experiments (MOJAVE) VLBI survey. Kovalev et al. (2005) reported that EGRET blazars in the 15 GHz MOJAVE survey were more compact than non-EGRET blazars. EGRET blazars have also been claimed to have much higher superluminal speeds than other blazars, and to have gamma-ray flares associated with the ejection of superluminal radio knots (Jorstad et al. 2001a, 2001b; Kellermann et al. 2004). However, in consideration of a larger sample (taken at 2 and 8 GHz) Piner et al. (2007) find no significant difference between the jet velocities of EGRET and non-EGRET blazars. In either case it still is unclear whether the radio flaring, or the ejection of new components, precedes or follows the gamma-ray flare, or whether there are in fact two classes of gamma-ray blazars (e.g., Sikora et al. 2001, 2002), one class with steep gamma-ray spectra and another class with flat gamma-ray spectra.

We have recently completed the 5 GHz VLBA Imaging and Polarimetry Survey (VIPS) of 1127 flat-spectrum sources stronger than 85 mJy in the northern cap region of the Sloan Digital Sky Survey (SDSS). VIPS (Taylor et al. 2005; Helmboldt et al. 2007b) was carried out between January and August of 2006 and includes 5 GHz, full-polarization images of 958 sources as well as 147 total intensity images for sources previously observed as part of the Caltech Jodrell Bank Flat spectrum (CJF) survey. The small remainder (22) were previously observed in the VIPS pilot survey and/or in the MOJAVE survey. Over 99% of the VIPS sources have been successfully imaged, with just under 1% being too weak to reliably self-calibrate and image.

The large, uniform sample provided by VIPS will have many uses, including enabling the intelligent follow-up of gamma-ray blazars as they flare and are detected by the *Gamma-Ray Large Area Space Telescope* (*GLAST*; Gehrels et al. 2001). *GLAST*, to be launched in early 2008, will provide a dramatic increase in the resolution and energy range and over 2 orders of magnitude increase in sensitivity over *CGRO* EGRET, thereby affording an unprecedented opportunity for the study of the centers of activity and jets in blazars in the gamma-ray energy range.

Here we make use of the VIPS survey to examine correlations in the parsec-scale jet properties of EGRET blazars.

2. SAMPLE DEFINITION

We have compared the latest EGRET catalog (Hartman et al. 1999) to the recently compiled Combined Radio All-Sky Targeted Eight GHz Survey (CRATES; Healey et al. 2007), and from the

[1] Department of Physics and Astronomy, University of New Mexico, 800 Yale Boulevard NE, Albuquerque, NM 87131.
[2] Department of Physics, Stanford University, Stanford, CA 94305.
[3] Naval Research Laboratory, Washington, DC 20375.
[4] Department of Physics, University of California at Davis, 1 Shields Avenue, Davis, CA 95616.
[5] National Radio Astronomy Observatory, P.O. Box O, Socorro, NM 87801.
[6] Astronomy Department, California Institute of Technology, MC 105-24, 1200 East California Boulevard, Pasadena, CA 91125.
[7] NASA Goddard Space Flight Center, Greenbelt, MD 20771.
[8] Kavli Institute for Particle Astrophysics and Cosmology (KIPAC), Stanford University, P.O. Box 20450, MS 29, Stanford, CA 94309.
[9] Department of Astrophysics, Denys Wilkinson Building, University of Oxford, Keble Road, Oxford OX1 3RH, UK.

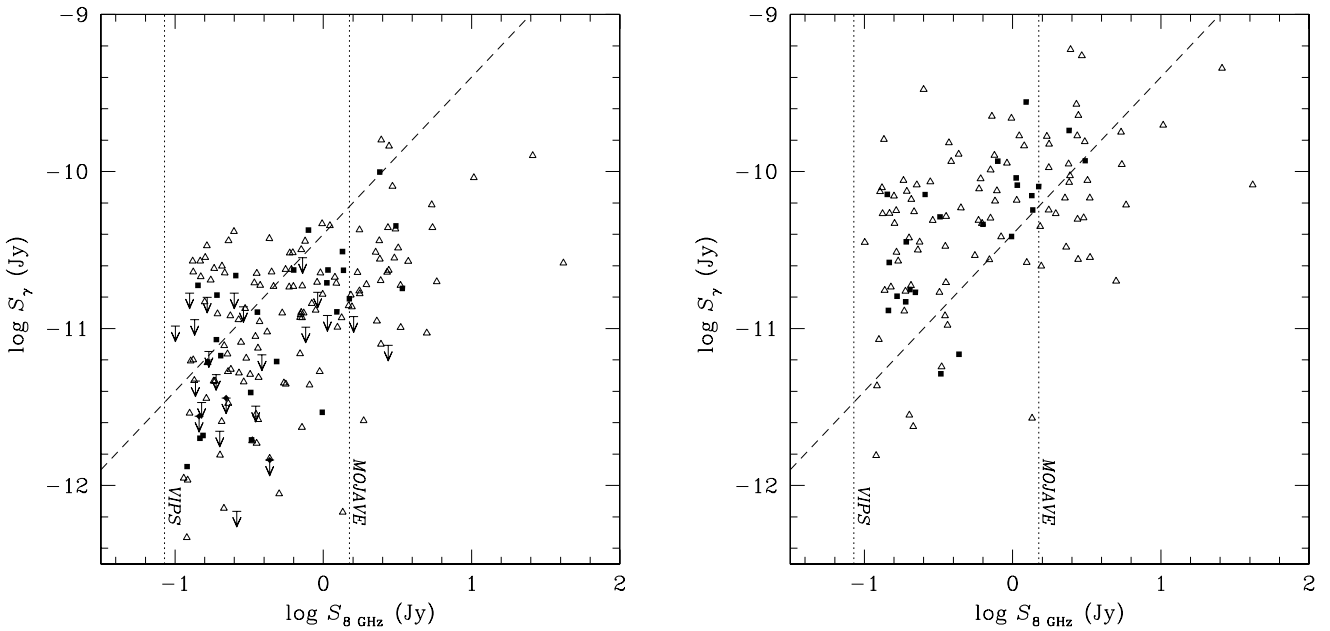

FIG. 1.—*Left*: Mean EGRET fluxes vs. the 8.4 GHz flux density. The mean fluxes are mission-averaged values from all four EGRET observing cycles, listed as "P1234" in the 3EG catalog. *Right*: Peak gamma-ray flux vs. radio flux density, where peak designates the largest flux from a single (typically 2 week long) EGRET viewing period, provided the detection significance exceeded 3 σ. The dashed line is not a fit to the data, but is only present to show that assuming gamma-ray flux proportional to the radio flux does not fit well at low radio flux densities; it appears that a statistically significant fraction of sub-jansky blazars may be bright in the gamma ray. Squares indicate VIPS sources discussed in this paper. The vertical dashed lines indicate the flux density limits of the VIPS and MOJAVE surveys assuming a flat spectrum (i.e., no correction has been made for spectral index effects).

intersection compiled a sample of 173 candidate EGRET sources at $|b| > 10^\circ$. In Figure 1 we plot the gamma-ray mean and peak fluxes against the 8.4 GHz radio flux density from CRATES (Healey et al. 2007) for 173 and 117 sources, respectively. The VIPS sample (which covers only ~14% of the sky), is derived from the Cosmic Lens All-Sky Survey (CLASS; Myers et al. 2003), but otherwise has similar radio flux limits and spectral selection as CRATES. Both CRATES and CLASS include A-configuration VLA observations at 8.4 GHz. The full radio/gamma-ray properties of the sample will be discussed in S. E. Healey et al. (2008, in preparation). Here we focus on the candidate EGRET sources within the ~5700 deg^2 region of the sky covered by VIPS, which provides uniform quality VLBI imaging. The results are summarized in Table 1. This list contains 12 VIPS sources deemed likely candidates, and 19 VIPS sources deemed plausible candidates. Here "likely" and "plausible" refer to ranges in the figure of merit (FoM). The FoM is computed based on the 8.4 GHz flux density, the radio spectral index, the X-ray flux density, and the positional coincidence (Sowards-Emmerd et al. 2003). A source is considered likely if it has FoM > 1, and plausible if it has $1.0 >$ FoM > 0.25.

In some cases multiple VIPS sources are assigned to a single EGRET source. Since some EGRET sources may be in fact composites of multiple blazars we have not made any distinction between sources with multiple identifications and those with a single identification. For six bright sources otherwise meeting the VIPS source criteria, MOJAVE observations are available. In Figure 2 we show the 5 GHz VIPS images or 15 GHz MOJAVE images for all 12 sources identified with EGRET blazars with high confidence (the likely candidates). In Figures 3 and 4 we show the images for 19 sources identified as plausible counterparts. For completeness we include 15 GHz MOJAVE images (Kellermann et al. 2004) for those six VIPS sources that were not imaged at 5 GHz. One should remember that due to the large range in redshifts, the individual rest-frame emitted frequencies can range over a factor up to 3.2.

3. MORPHOLOGICAL COMPARISON

While a number of radio-bright EGRET sources distributed over the sky have been imaged with VLBI (see references discussed in § 1), only in the VIPS region has the full EGRET candidate sample been uniformly imaged down to a flux density limit of 85 mJy at 8 GHz. In this section we examine the VLBI-scale properties of the 31 EGRET candidate blazars in this uniform sample, and for the 25 sources imaged as part of VIPS, we compare them to the properties of the VIPS survey of 1127 sources.

3.1. *Source Classes*

The classification of the EGRET candidates in VIPS is eight PS (point sources), three SJET (short jets), and 14 LJET (long jets) according to the automatic classification scheme of Helmboldt et al. (2007b; see Table 2). There are no CSO (compact symmetric object) candidates or CPLX (complex) sources. Applying the same classification rules to the six MOJAVE sources adds five LJET and one SJET for totals of eight (25%) PS, four (13%) SJET, and 19 (61%) LJET. This can be compared to the population in VIPS as a whole, which is 25% PS, 22% SJET, 43% LJET, 9% CSO, and 2% CPLX. If EGRET candidates were drawn from the VIPS population at random, then we would expect 8 ± 3 PS, 7 ± 3 SJET, 13 ± 4 LJET, and 3 ± 2 CSO and CPLX. While the number of PS and SJET sources are roughly as expected we find a marginally significant lack of CSOs, and a marginally significant excess of sources with long jets (LJET) on the parsec scale.

3.2. *Polarization*

Polarization is detected from all six of the MOJAVE sources and from nine of the 25 VIPS sources for a total of 48% $\pm$ 12%.

TABLE 1
EGRET Identifications

3EG Name (1)	VIPS Name (2)	$S_{8.4}$ (3)	α (4)	ΔTS (5)	FoM (6)	Code (7)	Mag (8)	z (9)	Type (10)	In CGRaBS? (11)
J0743+5447	J0742+5444	142.8	−0.387	0.517	0.502	!	17.3	0.723	FSRQ	...
J0808+5114	J0807+5117	358.8	0.280	0.359	7.241	!!!	17.6	1.136	FSRQ	CGRaBS
J0808+5114	J0809+5218	154.2	−0.103	2.398	1.186	!!!	14.5	0.138	BLL	...
J0829+2413	J0830+2410	793.7	0.027	0.701	7.009	!!!	16.3	0.940	FSRQ	CGRaBS
J0853+1941	J0854+2006	3414.9	0.443	1.519	7.872	!!!	15.6	0.306	BLL	CGRaBS
J0917+4427	J0920+4441	1368.3	0.153	7.051	0.470	!	16.5	2.190	FSRQ	CGRaBS
J0952+5501	J0957+5522	1498.9	−0.410	3.839	0.427	!	16.8	0.896	FSRQ	...
J1052+5718	J1058+5628	189.8	−0.115	5.490	0.387	!	14.6	0.144	BLL	CGRaBS
J1104+3809	J1104+3812	631.6	−0.109	1.126	6.582	!!!	13.0	0.031	BLL	CGRaBS
J1200+2847	J1159+2914	1233.3	−0.286	4.034	0.829	!	17.4	0.729	FSRQ	CGRaBS
J1222+2841	J1221+2813	1055.5	0.194	8.313	0.280	!	14.2	0.102	BLL	CGRaBS
J1224+2118	J1224+2122	1073.9	−0.383	1.445	1.522	!!!	16.0	0.435	FSRQ	...
J1227+4302	J1221+4411	435.2	−0.149	5.239	0.456	!	17.8	1.344	FSRQ	CGRaBS
J1227+4302	J1224+4335	220.8	−0.200	1.567	1.133	!!!	...	1.075	FSRQ	...
J1227+4302	J1226+4340	145.1	−0.141	1.367	0.866	!	18.5	1.999	FSRQ	...
J1323+2200	J1321+2216	323.6	0.010	5.353	0.509	!	19.4	0.943	FSRQ	CGRaBS
J1323+2200	J1322+2148	147.3	−0.288	3.400	0.261	!	19.1	1.680	FSRQ	...
J1323+2200	J1327+2210	984.0	0.073	6.547	0.381	!	18.8	1.400	FSRQ	CGRaBS
J1329+1708	J1331+1712	120.7	−0.233	1.454	0.425	!	17.2	...	BLL	...
J1329+1708	J1333+1649	483.8	0.106	3.072	1.982	!!!	16.4	2.097	FSRQ	CGRaBS
J1347+2932	J1343+2844	192.0	−0.127	5.069	0.336	!	16.5	0.908	FSRQ	...
J1424+3734	J1419+3821	775.8	0.120	5.408	0.840	!	19.2	1.831	FSRQ	CGRaBS
J1424+3734	J1421+3855	132.1	0.228	4.478	0.441	!	17.4	0.489	FSRQ	...
J1424+3734	J1426+3625	613.0	0.201	6.357	0.428	!	20.3	1.091	FSRQ	CGRaBS
J1605+1553	J1603+1554	256.9	0.524	2.483	4.280	!!!	12.1	0.109	FSRQ	CGRaBS
J1614+3424	J1613+3412	3088.1	−0.165	2.313	1.984	!!!	17.1	1.397	FSRQ	CGRaBS
J1635+3813	J1635+3808	2403.9	−0.085	1.488	3.599	!!!	17.2	1.814	FSRQ	CGRaBS
J1733+6017	J1722+5856	328.0	0.189	6.953	0.264	!	19.0	1.979	FSRQ	CGRaBS
J1733+6017	J1722+6105	203.2	0.141	3.932	0.911	!	19.4	2.058	FSRQ	CGRaBS
J1733+6017	J1724+6055	166.0	−0.042	2.340	0.827	!	...	...	...	...
J1738+5203	J1740+5211	1347.2	0.275	0.314	11.149	!!!	16.7	1.379	FSRQ	CGRaBS

Notes.—Col. (1): 3EG name based on EGRET coordinates. Col. (2): VIPS source name based on CLASS coordinates. Col. (3): 8.4 GHz flux density from CLASS. Col. (4): α is the spectral index ($S \sim \nu^{\alpha}$) between NVSS (NRAO VLA Sky Survey; Condon et al. 2007) at 1.4 GHz and CLASS at 8.4 GHz. Col. (5): "ΔTS" is a measure of the positional correspondence of the radio source to the peak of the gamma-ray flux. Lower values indicate a better positional correspondence (see Sowards-Emmerd et al. 2003). Col. (6): "FoM" is the figure of merit (Sowards-Emmerd et al. 2003). Col. (7): "Code" is a classification of the same type as in Sowards-Emmerd et al. (2003): sources with FoM > 1.0 were deemed "likely" counterparts (denoted by "!!!"), and sources with $0.25 <$ FoM < 1.0 were deemed plausible counterparts (denoted by "!"). Col. (8): The optical magnitude of the host galaxy. Col. (9): The redshift from Véron-Cetty & Véron (2006). Col. (10): Source classification, where FSRQ = flat-spectrum radio quasar and BLL = BL Lac object. Col. (11): An indication if the source is included in the CBRaBS sample (S. E. Healey et al. 2008, in preparation).

This is higher than the average of 36% ± 4% in VIPS overall (Helmboldt et al. 2007b), and the 41% ± 4% average for LJETs, although the numbers of sources involved are too small to make a definitive statement. Similarly a detailed examination of the polarization properties is handicapped by small-number statistics and the fact that we have a mix of 5 GHz measurements for VIPS sources and 15 GHz measurements for MOJAVE sources. Lister & Homan (2005) found that the jets (but not the cores) of EGRET blazars tended to have nearly twice the level of fractional polarization compared to MOJAVE sources not detected by EGRET, and are also more luminous. They attribute the difference to a higher mean Doppler factor for the EGRET blazars.

3.3. *Core Fraction*

In Figure 5 we plot the distribution of core-to-jet ratio (defined as the ratio of flux density at 5 GHz in the VLBI core compared to the jet emission from the source at 5 GHz) for the EGRET candidates against the distribution for the VIPS survey as a whole. No *k*-corrections have been applied, even though the difference in spectral index between the core and the extended emission will result in a change in the ratio with source redshift. Given the similar range in redshifts, and the core-dominated nature of the sources, the corrections should be modest and similar for both EGRET-detected blazars and VIPS sources as a whole. From the histograms, the EGRET sources appear to be biased toward more core-dominated systems. The K-S test probability that the two distributions were drawn from the same parent distribution is 4%. The core flux density for the EGRET blazars can be found in Table 3.

3.4. *Brightness Temperature*

We have obtained the brightness temperatures from automatic model fits to source components as described in Helmboldt et al. (2007b). For sources with two or fewer components we have further refined the our model fitting procedure by fitting to the visibility data directly. Only image plane model fitting was carried out in Helmboldt et al. (2007b) due to the tendency for the automatic visibility model fitting to go awry for complicated sources. The minimum observable size for each source was calculated using equation (2) from Kovalev et al. (2005), where we computed the signal-to-noise ratio of each core using the core flux density, the rms measured from the 5 GHz image, and a beam FWHM of 3 mas, the largest dimension of our restoring beam. For those sources where the estimated core size is less than this

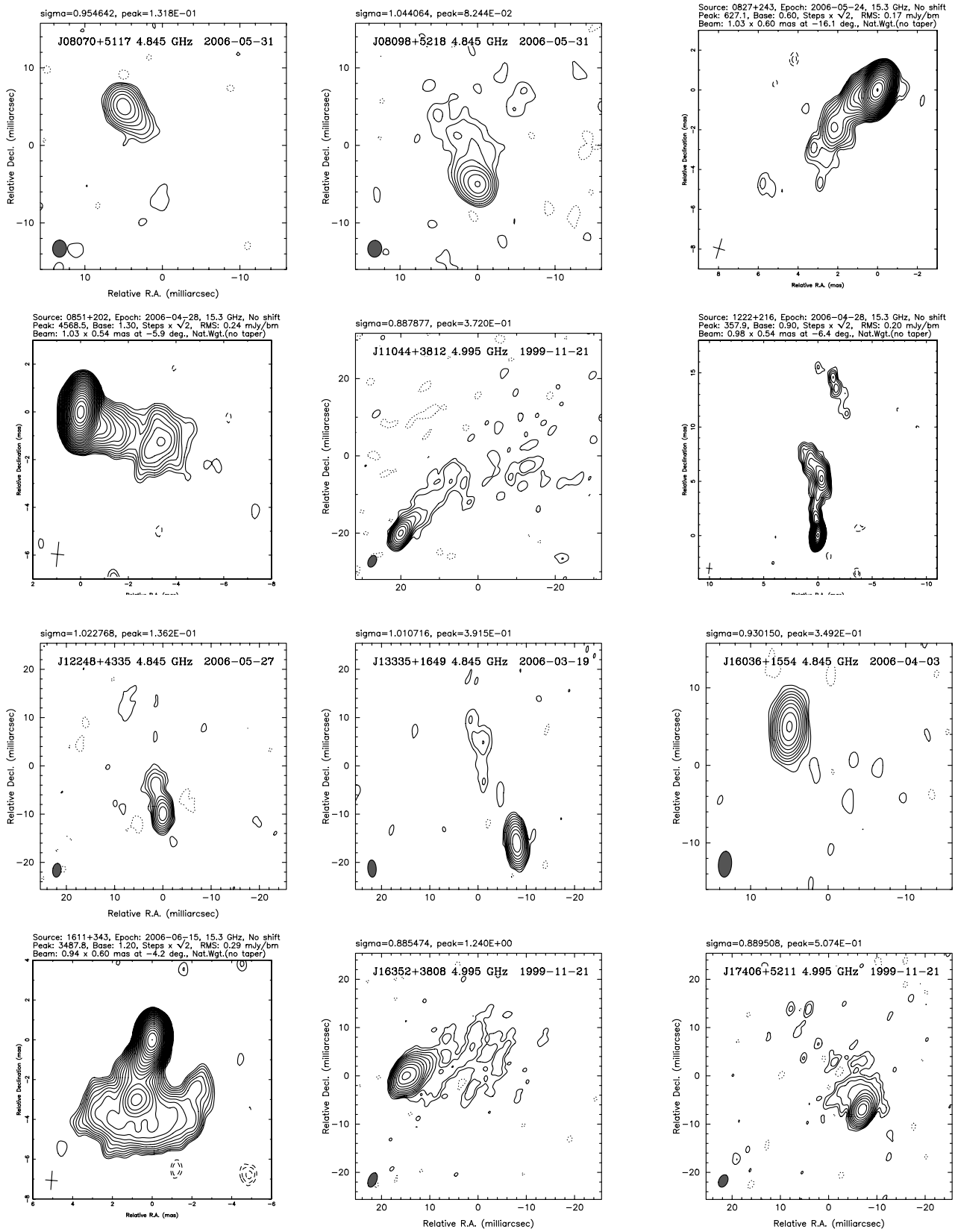

FIG. 2.—Images from VIPS and MOJAVE for 12 sources identified as likely EGRET candidates.

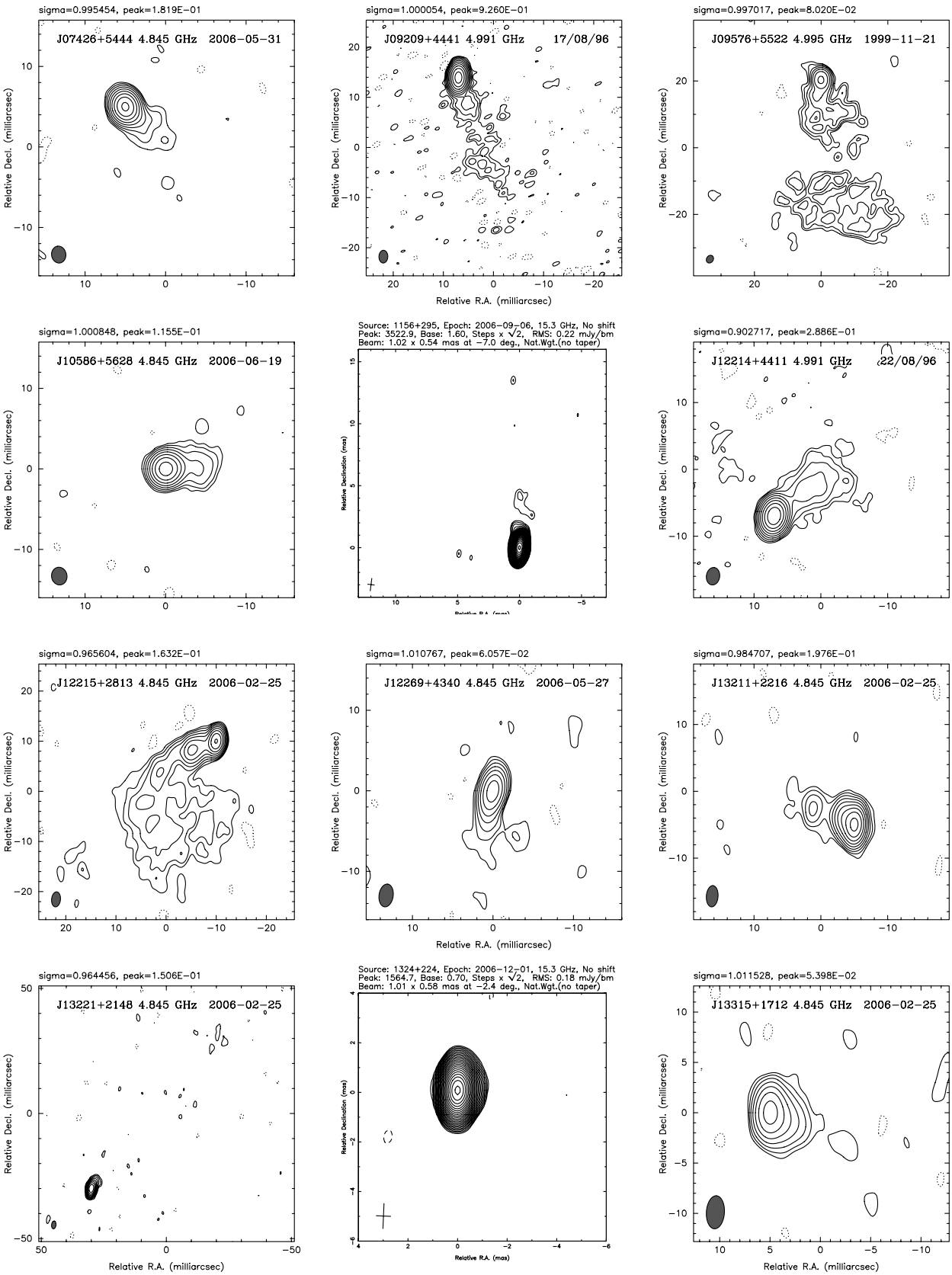

FIG. 3.—Images from VIPS and MOJAVE for 12 sources identified as plausible EGRET candidates.

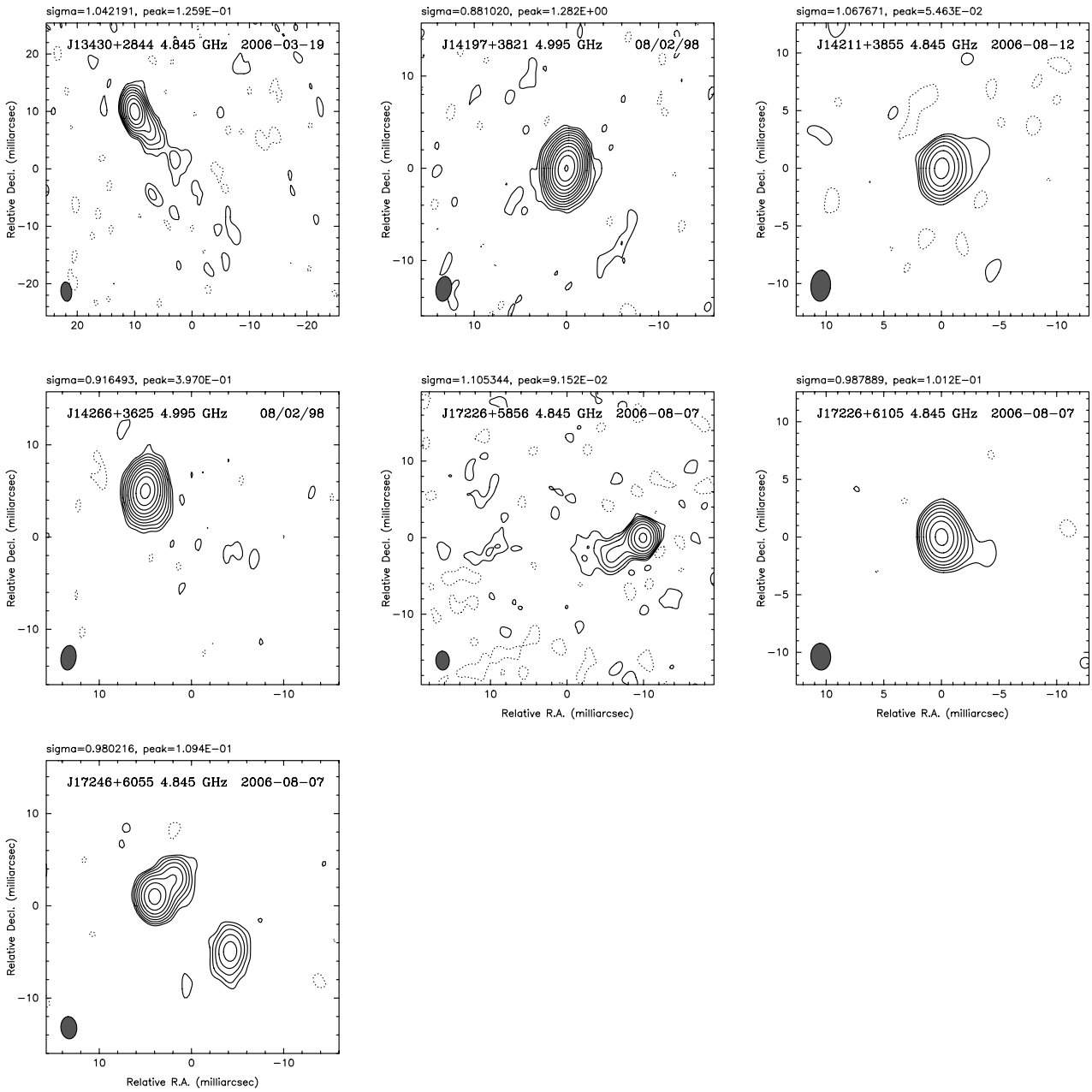

FIG. 4.—Images from VIPS and MOJAVE for seven sources identified as plausible EGRET candidates.

minimum size (∼10% of all VIPS sources), we used the minimum size to compute T_B. In Table 3 we provide the core sizes, core T_B, brightest jet component T_B, $\delta_P A$, and jet opening half-angle for the VIPS blazars. For sources where the estimated core FWHM is less than the minimum, the core diameter is preceded by a less than sign and the core temperature is preceded by a greater than sign. In all cases we compute the observed brightness temperatures, without any correction to the source rest frame.

There is some indication that the brightness temperature for the cores of the EGRET candidates may be higher than average (see distributions in Fig. 6). The K-S test probability for these two distributions coming from the same parent population is 4%. For the jet components (formally, the brightest jet component) the two distributions look fairly similar, except that the spread in the EGRET distribution is smaller (see lower panel of Fig. 6); the K-S test for this pair of distributions is 11%.

3.5. *Jet Opening Angle*

We have measured a mean opening half-angle by the following procedure: We measure the separation of each jet component from the core along the jet axis (taken to be a linear fit to the component positions) and the distance of each component from the jet axis, i.e., x' and y' positions in a rotated coordinate system with the jet axis along the x'-axis. For each component, we measure its extent from its center along a line perpendicular to the jet axis using the parameters of its elliptical fit, and then deconvolve this using the extent of the Gaussian restoring beam

TABLE 2
VIPS Source Properties

Source Number (1)	Source Name (2)	α (J2000.0) (3)	δ (J2000.0) (4)	UT Date (5)	$F_{8.5}$ (mJy) (6)	F_5 (mJy) (7)	$F_{5,\,\max}$ (mJy beam^{-1}) (8)	rms_5 (mJy beam^{-1}) (9)	N_{GC} (10)	T_a (11)	T_e (12)	$\overline{R}$ (mas) (13)	$D_{\max}$ (mas) (14)	P.A.$_{\mathrm{jet}}$ (deg) (15)
72	J08070+5117	08 07 01.0133	+51 17 38.670	2006 May 31	358.8	175.9	84.0	0.23	1	PS	...	1.3	...	...
78	J08098+5218	08 09 49.1899	+52 18 58.252	2006 May 31	154.2	125.6	56.1	0.25	2	LJET	...	3.4	6.7	20.2
402	J11044+3812	11 04 27.3145	+38 12 31.794	1999 Nov 21	631.6	421.4	372.0	0.34	3	LJET	...	9.6	23.8	−42.3
554	J12248+4335	12 24 51.5074	+43 35 19.276	2006 May 27	220.8	173.5	98.2	0.21	2	LJET	...	4.0	8.0	13.0
683	J13335+1649	13 33 35.7819	+16 49 04.027	2006 Mar 19	483.8	442.2	310.0	0.28	2	LJET	...	12.8	25.5	18.6
937	J16036+1554	16 03 38.0650	+15 54 02.378	2006 Apr 03	256.9	348.3	347.5	0.20	1	PS	...	1.2	...	...
994	J16352+3808	16 35 15.4931	+38 08 04.497	1999 Nov 21	2423.3	2201.9	1240.0	0.46	2	SJET	...	2.4	4.8	86.2
1102	J17406+5211	17 40 36.9805	+52 11 43.413	1999 Nov 21	1358.5	609.4	507.4	0.30	2	LJET	...	3.2	6.5	0.3
27	J07426+5444	07 42 39.7904	+54 44 24.679	2006 May 31	142.8	207.0	163.4	0.23	1	PS	...	1.2	...	...
214	J09209+4441	09 20 58.4599	+44 41 53.988	1996 Aug 17	1368.3	1173.5	926.0	0.71	2	LJET	...	4.2	8.5	−18.6
282	J09576+5522	09 57 38.1837	+55 22 57.740	1999 Nov 21	1498.9	563.2	80.2	1.99	4	LJET	...	19.1	55.9	19.6
387	J10586+5628	10 58 37.7261	+56 28 11.180	2006 Jun 19	189.8	149.4	86.1	0.22	2	LJET	...	3.5	7.0	−86.6
548	J12214+4411	12 21 27.0450	+44 11 29.667	1996 Aug 22	435.2	351.1	288.6	0.32	2	LJET	...	5.4	10.7	52.5
550	J12215+2813	12 21 31.6936	+28 13 58.497	2006 Feb 25	893.1	401.2	149.4	0.24	6	LJET	...	9.5	25.5	−44.3
556	J12269+4340	12 26 57.9051	+43 40 58.438	2006 May 27	145.1	77.8	44.0	0.23	2	LJET	...	3.2	6.4	−8.2
655	J13211+2216	13 21 11.2041	+22 16 12.098	2006 Feb 25	323.6	253.1	160.9	0.19	2	SJET	...	2.3	4.7	58.2
656	J13221+2148	13 22 11.3989	+21 48 12.268	2006 Feb 25	147.3	171.0	131.9	0.21	1	PS	...	1.2	...	...
679	J13315+1712	13 31 33.4457	+17 12 50.615	2006 Feb 25	120.7	66.3	41.6	0.21	2	SJET	...	2.5	5.0	−113.4
697	J13430+2844	13 43 00.1805	+28 44 07.492	2006 Mar 19	192.0	153.2	99.3	0.24	2	LJET	...	3.2	6.5	−140.9
754	J14197+3821	14 19 46.6162	+38 21 48.485	1998 Feb 08	775.8	1318.1	1282.0	0.23	1	PS	...	1.1	...	...
758	J14211+3855	14 21 06.0337	+38 55 22.829	2006 Aug 12	132.1	54.4	49.8	0.20	1	PS	...	1.1	...	...
769	J14266+3625	14 26 37.0861	+36 25 09.576	1998 Feb 08	613.0	432.9	397.0	0.22	1	PS	...	1.1	...	...
1073	J17226+5856	17 22 36.7292	+58 56 22.265	2006 Aug 07	328.0	111.9	66.3	0.27	2	LJET	...	3.5	6.9	−60.8
1074	J17226+6105	17 22 40.0595	+61 05 59.802	2006 Aug 07	203.2	105.8	96.6	0.19	1	PS	...	1.2	...	...
1082	J17246+6055	17 24 41.4172	+60 55 55.746	2006 Aug 07	166.0	157.4	91.7	0.28	3	LJET	...	5.8	12.7	−131.2

Notes.—Col. (1): VIPS source number. Col. (2): VIPS source name. Col. (3): Right ascension (J2000.0). Col. (4): Declination (J2000.0). Units of right ascension are hours, minutes, and seconds, and units of declination are degrees, arcminutes, and arcseconds. Col. (5): UT date of the observations. Col. (6): The flux density at 8.5 GHz from the CLASS survey. Col. (7): The total cleaned flux density from the 5 GHz VLBA map. Col. (8): The peak flux density from the 5 GHz VLBA map. Col. (9): The rms noise of the 5 GHz VLBA image. Col. (10): The number of dominant Gaussian components (i.e., that contain more than 95% of the total flux) fit to the 5 GHz VLBA map (see § 2.3 of Helmbolt et al. 2007a). Col. (11): The source type derived from the automated Gaussian component classification (see § 2.3 of Helmbolt et al. 2007a). Col. (12): The source type determined by visual inspection of the *I* image for sources where the "by eye" and automatic classifications disagree. Col. (13): The mean radius (i.e., mean distances from the mean component position) for the ensemble of dominant Gaussian components. Col. (14): The maximum separation among the dominant Gaussian components. Col. (15): The jet position angle (measured from north through east).

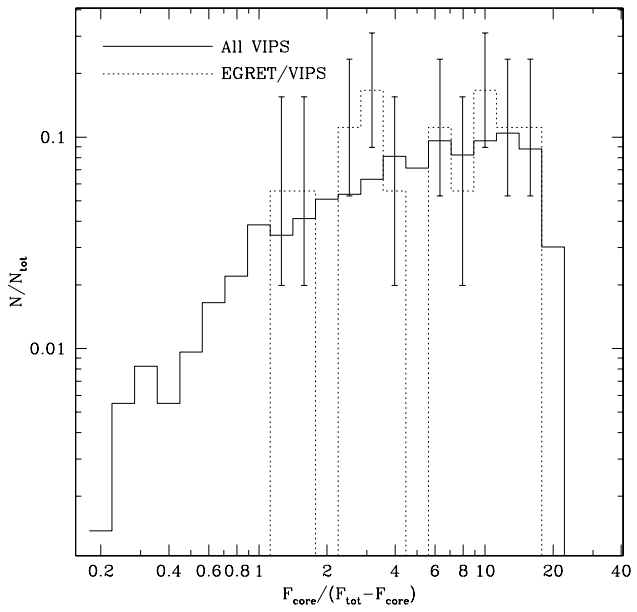

FIG. 5.—Distribution of the 5 GHz ratio of core-to-jet flux density: $R = F_{\rm core}/(F_{\rm tot} - F_{\rm core})$, where $F_{\rm tot}$ is the total flux density at 5 GHz, for EGRET candidates and for VIPS as a whole. No *k*-correction has been made (see text).

along the same line. The opening half-angle measured from each component is then taken to be

$$\psi = \arctan[(|y'| + dr)/|x'|],$$

where *dr* is the deconvolved Gaussian size perpendicular to the jet axis. After measuring this for each jet component, we average them to get one value. This is only done for sources with more than two total components (i.e., at least two jet components). This means that, as in the case of jet bending (see § 3.6), we only have quantitative estimates for four of the EGRET/VIPS sources (see. Fig. 7). Although this is based on very small statistics, there is a hint that EGRET/VIPS jets have unusually large opening angles. We find three sources have jet opening half-angles exceeding the VIPS median (18.9°). Monte Carlo simulations of opening angles using the VIPS sample suggest that three out of four of the randomly sampled values are greater than the median about 30% of the time. So, there is less than a 1 in 3 chance that the EGRET blazars have the same distribution for the opening angle as the whole VIPS sample. Looking at the EGRET/MOJAVE and EGRET/VIPS sources by eye in Figures 2–4 strengthens this impression. We see in Figures 2–4 six sources (J08098+5218, J09576+5522, J12215+2813, 1611+343, J16352+3808, and J17406+5211) that have opening angles larger than 20°. This can be compared to the VIPS images for the survey as a whole, which are online.[10] In a few of the blazars the

[10] See http://www.phys.unm.edu/~gbtaylor/VIPS/.

TABLE 3
BRIGHTNESS TEMPERATURES OF VIPS BLAZARS

Source Number (1)	Source Name (2)	$F_{5,\rm core}$ (mJy) (3)	$D_{\rm core}$ (mas) (4)	$T_{B,\rm core}$ (K) (5)	$T_{B,\rm jet}$ (K) (6)	ΔP.A. (deg) (7)	Ψ (deg) (8)
72	J08070+5117	175.9	0.942	9.70×10^9	...	...	...
78	J08098+5218	108.9	1.050	4.83×10^9	1.56×10^7	...	...
402	J11044+3812	370.2	0.291	2.13×10^{11}	3.59×10^7	−0.62	15.07
554	J12248+4335	156.9	0.653	1.80×10^{10}	3.37×10^7	...	...
683	J13335+1649	417.9	0.538	7.05×10^{10}	9.97×10^6	...	...
937	J16036+1554	348.3	<0.121	$>1.16 \times 10^{12}$	...	...	...
994	J16352+3808	2013.7	1.999	2.47×10^{10}	2.74×10^8	...	...
1102	J17406+5211	574.7	0.700	5.75×10^{10}	4.09×10^7	...	...
27	J07426+5444	207.0	0.439	5.26×10^{10}	...	...	...
214	J09209+4441	1080.4	0.785	8.58×10^{10}	5.19×10^7	...	...
282	J09576+5522	127.3	7.206	1.20×10^8	7.96×10^7	−32.94	60.29
387	J10586+5628	129.6	0.817	9.49×10^9	2.10×10^7	...	...
548	J12214+4411	303.6	0.528	5.33×10^{10}	2.63×10^7	...	...
550	J12215+2813	177.5	0.614	2.30×10^{10}	1.62×10^8	−11.50	27.45
556	J12269+4340	72.9	0.578	1.07×10^{10}	1.54×10^7	...	...
655	J13211+2216	227.7	0.780	1.83×10^{10}	6.51×10^7	...	...
656	J13221+2148	171.0	0.465	3.87×10^{10}	...	...	...
679	J13315+1712	61.0	0.788	4.80×10^9	1.86×10^7	...	...
697	J13430+2844	137.3	0.602	1.85×10^{10}	3.20×10^7	...	...
754	J14197+3821	1318.1	0.242	1.10×10^{12}	...	...	...
758	J14211+3855	54.4	<0.304	$>2.88 \times 10^{10}$	...	...	...
769	J14266+3625	432.9	0.503	8.36×10^{10}	...	...	...
1073	J17226+5856	97.2	0.574	1.44×10^{10}	2.26×10^7	...	...
1074	J17226+6105	105.8	0.224	1.03×10^{11}	...	...	...
1082	J17246+6055	121.5	0.604	1.63×10^{10}	6.71×10^7	−89.59	30.91

NOTES.—Col. (1): VIPS source number. Col. (2): VIPS source name. Col. (3): The 5 GHz flux density of the core. Col. (4): The FWHM of the core component estimated using a circular Gaussian fit to the visibility data. Col. (5): The mean brightness temperature of the core. Col. (6): The mean brightness temperature of the brightest component outside the core. Col. (7): The difference between the outer and inner position angles of the jet for sources with more than two jet components. Col. (8): The jet opening half-angle for sources with more than two jet components.

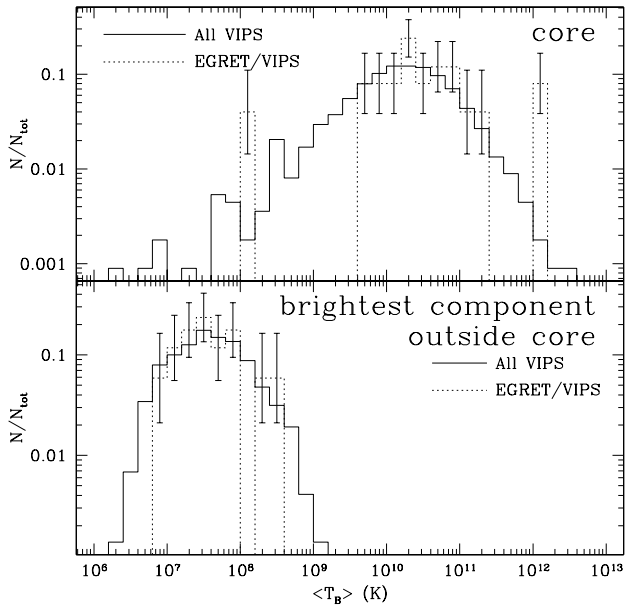

FIG. 6.—Distribution of the brightness temperature, T_b, for EGRET candidates and for VIPS as a whole.

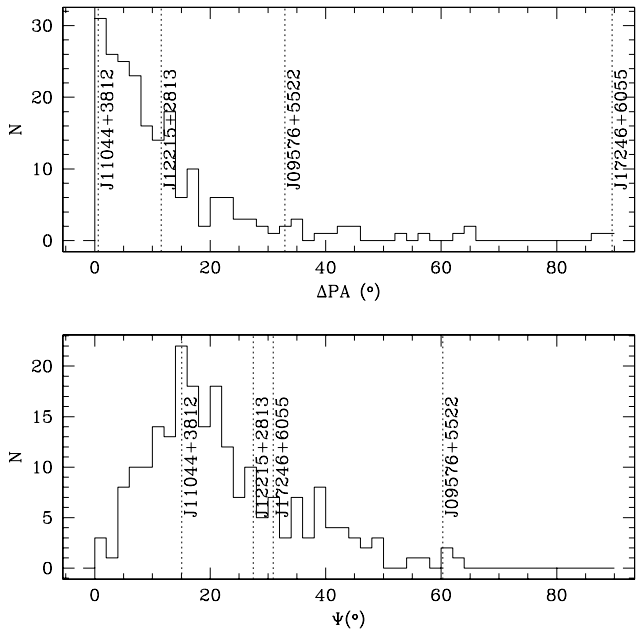

FIG. 7.—Distributions of the opening angle of the jet, and of the parsec-scale bending of the jet for VIPS as a whole. The angles for four EGRET sources are marked and labeled.

emission is rather diffuse, which is why they do not show up in the automatic opening angle calculation.

3.6. *Jet Bending and Length*

We can also compare the amount of bending in the jet on the parsec scale for the EGRET candidates compared to VIPS as a whole. The amount of bending was calculated by fitting a parabola to the centroids of Gaussian model components (Helmboldt et al. 2007a). Again we are limited to only four sources (Fig. 7), and the results are inconclusive. In fact, the source with the largest reported bend, J09576+5522, could be much less bent depending on whether the morphology is attributed to a twisting jet, or to a jet with a broad opening angle. Looking at the EGRET/MOJAVE and EGRET/VIPS sources by eye only increases the number of highly bent jets by one. We see in Figures 2–4 four sources (J12215+2813, J17226+5856, J17246+6055, and J17406+5211) that appear to bend through more than 20° on the parsec scale.

Given the slight preponderance of sources with long jets, we compared the distribution of jet length in EGRET blazars with VIPS as a whole. There does not appear to be an appreciable difference between the two populations. The K-S probability that the two are drawn from the same distribution is 34%.

4. NOTES ON INDIVIDUAL SOURCES

J11044+3812 (Mrk 421).—A well-known BL Lac and also one of the first sources to be detected in TeV emission (Punch et al. 1992). Mrk 421 was included in both the CJF (Taylor et al. 1994, 1996) and 2 cm surveys (Kellermann et al. 2004), and has also been recently imaged by Giroletti et al. (2006).

J16036+1554.—This source is completely unresolved by the VLBA observations at 5 GHz (Helmboldt et al. 2007b), and can be well fit with a single component (the core) with size of <0.12 mas. This results in a brightness temperature of $>1 \times 10^{12}$ K. Such completely unresolved sources without any jet components are quite rare—there are essentially no sources this compact in MOJAVE (Kovalev et al. 2005) or CJF (Taylor et al. 1994, 1996).

J17246+6055.—The faint (r-band magnitude 21.2) host galaxy does not yet have a known redshift or spectroscopic classification. The parsec-scale radio structure (see Fig. 4) is quite unusual with a core jet and a fairly compact component to the southeast. It is possible that this source could be a compact supermassive binary black hole, and further VLBI observations are in progress to test this hypothesis. Another possible explanation is a jet with a sharp bend and wide opening angle, such as Mrk 501 (Giroletti et al. 2004) or Mrk 421 (Giroletti et al. 2006; and see Fig. 2).

5. DISCUSSION

From an analysis of the properties of the EGRET candidates in § 4, we find that candidates tend to have high core fractions and high brightness temperatures. These facts support models wherein the gamma rays are produced in a jet oriented at a small angle to the line of sight (e.g., Dermer et al. 1992). The large opening angles seen in six out of the 31 sources could also indicate a sight line close to or within the beaming cone of the radio emission. A selection effect of this sort would happen naturally if the gamma rays are more tightly beamed or collimated than the radio. In other words, gamma-ray-selected sources have higher Doppler factors than the population of compact sources as a whole. This can also explain the observations of higher core fractions, higher brightness temperatures, and higher polarization in gamma-ray blazars compared to the population of active galactic nuclei (AGNs) as a whole, as well as the reports of faster motions. An unbiased comparison of jet components between the EGRET blazars and the VIPS sample at large supports this, although only four of the EGRET/VIPS sources have enough jet components to permit the unbiased (automatic) analysis so the statistics are poor.

Somewhat more surprising is the evidence in support of long jets, although this is of marginal significance. Continuing the line of discussion above that EGRET blazars have higher Doppler factors due to small angles to the line of sight, the a priori prediction, assuming jets of a fixed length and modest velocity, would be for shorter jets due to projection. Obtaining longer jets might

be possible if the jets of blazars have intrinsically greater surface brightness, or are highly Doppler boosted compared to sources in radio-selected samples. Longer jets in blazars could also be obtained if there is a bias in the selection. The redshift distribution for the VIPS sample is still incomplete, so it is difficult to investigate possible selection bias at this time. Given the weakness of the evidence, especially when comparing the distributions of jet lengths (§ 3.6), further speculation on this topic is not yet warranted.

6. CONCLUSIONS

Sources selected on the basis of their gamma-ray flux as determined by EGRET appear to have higher Doppler factors than the radio-selected population at large. In the VIPS survey this selection manifests itself in larger core fractions, higher core brightness temperatures, increased polarization, and possibly broader jets.

GLAST, which will launch in early 2008, will detect several thousand (Gehrels & Michelson 1999) of the tens of thousands of compact, radio-loud, flat-spectrum AGNs currently known. Confirming the tighter beaming angle for the gamma rays should be easily achieved with the improved statistics. Greater advances in understanding are anticipated, although detailed studies including multiwavelength flux monitoring, and multifrequency, multiepoch VLBI polarimetry will be possible only for a small subset of objects. As we have shown, the gamma-ray flux density is not simply related to the radio flux density, so selecting the brightest radio sources for study may not maximize the chances of coincidence with strong gamma-ray emission. Therefore it may be advantageous to consider selecting sources with large core fractions, high central brightness temperatures, and large opening angles, as well as strong radio flux density. *GLAST* could also see new populations of AGNs including Seyfert galaxies, and low-power radio galaxies. For this reason it is important to provide contemporaneous ground-based monitoring of a range of source classes, powers, and morphologies. Comparisons between the parsec-scale radio structures as revealed by VLBI observations and the time-variable gamma-ray flux, could discriminate between various models describing the production of the gamma-ray emission, or reveal that more than one mechanism is at work.

We thank an anonymous referee for constructive suggestions. The National Radio Astronomy Observatory is a facility of the National Science Foundation operated under cooperative agreement by Associated Universities, Inc.

REFERENCES

Condon, J. J., Cotton, W. D., Greisen, E. W., Yin, Q. F., Perley, R. A., Taylor, G. B., & Broderick, J. J. 1998, AJ, 115, 1693
Dermer, C. D., Schlickeiser, R., & Mastichiadis, A. 1992, A&A, 256, L27
Gehrels, N., & Michelson, P. 1999, Astropart. Phys., 11, 277
Gehrels, N., et al. 2001, in The Nature of Unidentified Galactic High-Energy Gamma-Ray Sources, ed. A. Carramiñana, O. Reimer, & D. J. Thompson (Dordrecht: Kluwer), 321
Giroletti, M., Giovannini, G., Taylor, G. B., & Falomo, R. 2006, ApJ, 646, 801
Giroletti, M., et al. 2004, ApJ, 600, 127
Hartman, R. C., et al. 1999, ApJS, 123, 79
Healey, S. E., et al. 2007, ApJS, 171, 61
Helmboldt, J. F., Taylor, G. B., Blandford, R. D., & Walker, R. C. 2007a, ApJ, 658, 203
———. 2007b, ApJ, submitted
Jorstad, S. G., Marscher, A. P., Mattox, J. R., Wehrle, A. E., Bloom, S. D., & Yurchenko, A. V. 2001a, ApJS, 134, 181
Jorstad, S. G., et al. 2001b, ApJ, 556, 738
Kellermann, K. I., et al. 2004, ApJ, 609, 539
Kovalev, Y. Y., et al. 2005, AJ, 130, 2473
Lähteenmäki, A., & Valtaoja, E. 2003, ApJ, 590, 95
Lister, M. L., & Homan, D. C. 2005, AJ, 130, 1389
Marscher, A. P. 2006, in AIP Conf. Proc. 856, Relativistic Jets: The Common Physics of AGN, Microquasars, and Gamma-Ray Bursts, ed. P. A. Hughes & J. N. Bregman (Melville: AIP), 1
Myers, S. T., et al. 2003, MNRAS, 341, 1
Piner, B. G., Mahmud, M., Fey, A. L., & Gospodinova, K. 2007, AJ, 133, 2357
Punch, M., et al. 1992, Nature, 358, 477
Reich, W., Steppe, H., Schlickeiser, R., Reich, P., Pohl, M., Reuter, H. P., Kanbach, G., & Schonfelder, V. 1993, A&A, 273, 65
Sikora, M., Blazejowski, M., Begelman, M. C., & Moderski, R. 2001, ApJ, 554, 1
Sikora, M., Blazejowski, M., Moderski, R., & Madejski, G. M. 2002, ApJ, 577, 78
Sowards-Emmerd, D., Romani, R. W., & Michelson, P. F. 2003, ApJ, 590, 109
Sowards-Emmerd, D., Romani, R. W., Michelson, P. F., & Ulvestad, J. S. 2004, ApJ, 609, 564
Sowards-Emmerd, D., et al. 2005, ApJ, 626, 95
Taylor, G. B., Vermeulen, R. C., Pearson, T. J., Readhead, A. C. S., Henstock, D. R., Browne, I. W. A., & Wilkinson, P. N. 1994, ApJS, 95, 345
Taylor, G. B., Vermeulen, R. C., Readhead, A. C. S., Pearson, T. J., Henstock, D. R., & Wilkinson, P. N. 1996, ApJS, 107, 37
Taylor, G. B., et al. 2005, ApJS, 159, 27
Urry, C. M., & Padovani, P. 1995, PASP, 107, 803
Véron-Cetty, M.-P., & Véron, P. 2006, A&A, 455, 773